In Situ Observation on Lime Dissolution in Molten Metallurgical Slags – Kinetic Aspects

ARTICLE *in* INDUSTRIAL & ENGINEERING CHEMISTRY RESEARCH · APRIL 2014

Impact Factor: 2.59 · DOI: 10.1021/ie500070h

5 AUTHORS, INCLUDING:

Z.H.I. Sun

Delft University of Technology

34 PUBLICATIONS **136** CITATIONS

SEE PROFILE

Joris Van Dyck

University of Leuven

15 PUBLICATIONS **90** CITATIONS

SEE PROFILE

Muxing Guo

University of Leuven

16 PUBLICATIONS **82** CITATIONS

SEE PROFILE

Bart Blanpain

University of Leuven

300 PUBLICATIONS **3,506** CITATIONS

SEE PROFILE

I&EC research
Industrial & Engineering Chemistry Research

Article

pubs.acs.org/IECR

In Situ Observation on Lime Dissolution in Molten Metallurgical Slags – Kinetic Aspects

X. Guo, Z. H. I. Sun,* J. Van Dyck, M. Guo,* and B. Blanpain

Department of Metallurgy and Materials Engineering, KU Leuven, B-3001 Leuven, Belgium

Ⓦ *Web-Enhanced Feature* Ⓢ *Supporting Information*

ABSTRACT: The chemical dissolution of lime particles in molten $CaO–Al_2O_3–SiO_2$-based slags was observed by using a confocal scanning laser microscope (CSLM) in a temperature range from 1450 to 1600 °C. The dissolution behavior was found to be largely dependent on temperature and slag chemistry. A considerable increase in the dissolution rate was observed at elevated temperatures. The *in situ* observations revealed that the dissolution process in the slags containing MgO was controlled by chemical reactions at the interface. For slags without MgO, the dissolution could be divided into three stages when an interfacial reaction (IR) layer formed at the interface. The dissolution was limited by chemical reactions during the early stage, a mixed control of product layer and boundary layer diffusion during the intermediate stage, and boundary layer diffusion control in the final stage. The IR layer formed during dissolution at the interface between the lime particles, and the liquid slag free of MgO was clearly a kinetic barrier for dissolution. A dissolution factor was defined to evaluate the dissolution mechanisms quantitatively by coupling the resistance and the driving forces of dissolution in different slags. This factor provided direct evidence that the addition of MgO in $CaO–Al_2O_3–SiO_2$ slags is beneficial for lime dissolution.

1. INTRODUCTION

During primary steelmaking, for example, basic oxygen furnace (BOF) and electric arc furnace (EAF) processes, lime and/or dolomite are employed as fluxes to obtain a basic slag and to help with the removal of harmful impurities such as sulfur and phosphorus.[1−3] Rapid and complete dissolution of lime into molten slag is required to ensure its effective utilization. Therefore, a better understanding of the lime dissolution mechanisms is of significant importance for process optimization. Lime dissolution is a complex process that may depend on the interface reaction rate, mass transfer condition, and slag properties. The mineralogical properties, for example, porosity and surface energy of the lime, were also found to influence the dissolution.[2,4−6] Determination of the rate-controlling step(s) is crucial in understanding the dissolution mechanisms. Traditional high temperature experiments in a resistance furnace are frequently used to study dissolution kinetics in molten slags.[5−7] The dissolution methods include a rotating lime cylinder,[4,5] rotating lime pellet or disk,[6] and static dissolution using a lime crucible.[2] However, these methods are intrinsically indirect observation. A large sample diameter (e.g., several centimeters) is usually used to ensure easier experimental operations where the detected lime dissolution is limited to be superficial and information after the intermediate stage of lime dissolution is not readily available. Moreover, the samples break easily with a rotating lime cylinder, and the local situation is changed that would make it difficult to obtain accurate information on the dissolution process.[8]

High temperature confocal scanning laser microscopy (CSLM) enables a superior solution to the experimental problems during lime dissolution by providing direct observation of the dissolution behavior of micrometer-sized lime particles into molten metallurgical slags. The dissolution details can be promptly recorded from the accumulation stage to the final stage of the dissolution. A quantitative evaluation of the dissolution rate becomes therefore possible. By further combining the CSLM observation with kinetic and thermodynamic calculations, the effects of the temperature and slag composition on the lime dissolution can be systematically interpreted. CSLM has been used in other studies, such as inclusion behavior in metal melts,[9] phase transformations,[10] and also dissolution of oxide particles such as magnesia, alumina, zirconia, and spinel into slags;[9,11,12] the *in situ* observation has been a great advantage. In our previous research,[13] the phase transformations during lime dissolution as well as the formation nature of an interfacial reaction (IR) layer between the lime particle and the liquid slag free of MgO were studied by using the CSLM technique. The present research focuses on the kinetic aspects of lime dissolution into $CaO–Al_2O_3–SiO_2$-based slags, aiming to identify (i) the significant factors influencing the dissolution and (ii) interactions between the driving forces and resistances and also (iii) to highlight the importance of MgO addition to accelerate lime dissolution for metallurgical applications.

2. MATERIALS AND EXPERIMENTS

2.1. Materials. The slags used in the experiments consisted of Al_2O_3, SiO_2, and CaO with or without MgO. The oxides used during the experiments were produced by Alfa Aesar, all with purities of 99.95 wt %. They were prepared by blending the pure oxide compounds in a mortar and filling into a molybdenum crucible. Before mixing, all the oxides were dried in a muffle furnace at 300 °C for 24 h. The crucible was placed

Received: January 8, 2014
Revised: March 26, 2014
Accepted: March 27, 2014
Published: March 27, 2014

   dx.doi.org/10.1021/ie500070h | *Ind. Eng. Chem. Res.* 2014, 53, 6325−6333

Table 1. Compositions (wt %) of the Slags Used in This Study

slag number	CaO	SiO_2	Al_2O_3	MgO	basicity (CaO/SiO_2)	basicity ($CaO+MgO/SiO_2$)
SM01	45.0	45.0	10.0	0	1.0	1.0
SM02	30.0	60.0	10.0	0	0.5	0.5
SM03	40.0	40.0	20.0	0	1.0	1.0
SM04	26.7	53.3	20.0	0	0.5	0.5
SM1	40.0	40.0	10.0	10.0	1.0	1.3
SM2	26.7	53.3	10.0	10.0	0.5	0.7
SM3	35.0	35.0	20.0	10.0	1.0	1.3
SM4	23.3	46.7	20.0	10.0	0.5	0.7

in a tube furnace under purified argon atmosphere and held for at least 24 h at a temperature of 1600 °C. Scanning electron microscopy analyses were applied to confirm the homogeneity of the as-obtained slags. As soon as this melting finished, the slags were quenched on a steel plate and crushed into small particles, which were then remelted in the CSLM to release any trapped argon before running an experiment. The compositions of the premelted slags are listed in Table 1, which is the same as our previous research.[13] The lime particles for dissolution were also produced by Alfa Aesar and prepared from coarse lime grains. Before dissolution, the particles were dried in a muffle furnace at 600 °C for 24 h to remove water.

2.2. Experimental Apparatus and Procedures. The CSLM-IIF equipment (CSLM coupled with Infrared Image Furnace, Lasertec, 1LM21M-SVF17SP) was used for *in situ* observations of lime dissolution at high temperatures. A detailed description of the CSLM can be found in previous work.[13] The interior surface of the furnace is gold plated and ellipsoidal in shape. The crucible is placed at the upper focal point of the elliptical heating chamber, and a halogen heating lamp is located at the lower focal point. The temperature is controlled by a B-type thermocouple (Pt-30 wt % Rh/Pt-6 wt % Rh) welded to the bottom of the sample holder. HiTOS software connected with a REX-P300 controller is used to program the temperature profiles. In order to ensure the accuracy of the measured temperature, calibration was performed using standard pure metal samples, for example, copper, nickel, palladium, and iron, prior to the lime dissolution experiments (see Figure 1S, Supporting Information, for more information).

Experimental procedures were kept the same as in our previous work.[13] Before the dissolution experiments, the heating chamber was evacuated to about 10 Pa and refilled with ultrapurified argon gas at least three times. The argon gas passed through a Restek triple filter for oxygen, moisture, and hydrocarbons and a Restek high capacity oxygen scrubber before entering the chamber. The slag sample with a lime particle on the surface was heated to the desired temperature. Evaluation of the lime dissolution always started from the point where the set temperature was reached. In order to reduce the interaction of the slag and the particle before the slag melting, the sample was heated at a relatively high rate of around 200−350 °C/min. For each slag (Table 1), the dissolution experiments were performed at temperatures of 1450, 1500, 1550, and 1600 °C. During the experiments, the uncertainty of temperature measurement is within ±2 °C. In the present investigation, the lime particles were of irregular shape. In order to evaluate the changes in lime particle size during the dissolution, a border was constructed by using image processing software around the lime particle in the images obtained via the HiTOS software (Figure 1). An equivalent radius was computed based on the measured projected area of the particle, and information on the dissolution kinetics was derived from the size change of the lime particle.

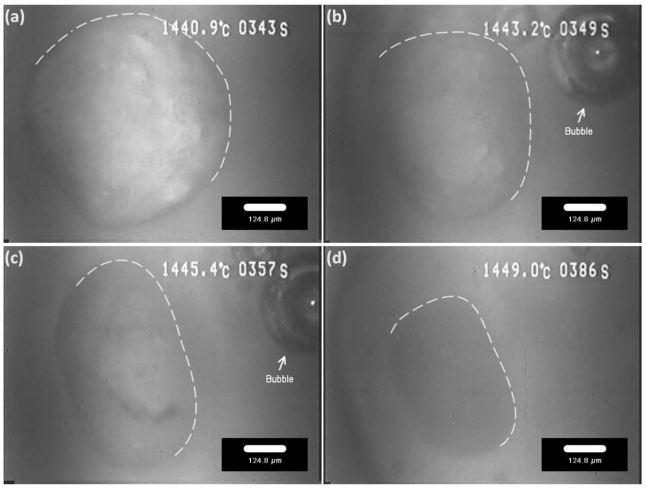

Figure 1. CSLM images of dissolution of CaO in slag SM4 at 1450 °C.

3. RESULTS AND DISCUSSION

3.1. Particle Size Evolution during Lime Dissolution. Figure 1 shows a typical lime dissolution in slag SM4 at 1450 °C. The area surrounded by a dashed line is considered as the particle size (Figure 1). During the dissolution, release of bubbles (Figure 1b and c) and rotation of the particle (see Movie 1) were observed. The bubbles are probably generated by the trapped air in the lime particle. The rotation is believed to result from a compositional buildup of CaO in the slag near the particle surface. During dissolution, a change in the local radius may result in local mass fluxes.[14] When the particle is not spherical, the mass fluxes vary at different positions of the particle surface inducing potential liquid flow in the boundary layer, and rotation of the particle can arise. This introduces fluctuations in the measurement of the particle size and will probably influence the shape of the radius evolution profile. The equivalent radius was calculated by assuming that the particle was a sphere, and therefore, the irregular shape of the particle is an important source of scatters in the dissolution curves. An example is given in Figure 2, and fluctuation of particle size happened during dissolution, which is indicated by the peaks in the radius evolution profile. However, these errors do not influence the overall tendency of the dissolution profiles and have little effect on the dissolution mechanism.

3.2. Interfacial Reaction (IR) Layer Formation during Lime Dissolution. An obvious IR layer could be observed during CaO dissolution experiments in MgO-free slags, as shown in Figure 3 (indicated by arrows).[13] The visibility of the layer depends on the temperature and slag compositions

dx.doi.org/10.1021/ie500070h | Ind. Eng. Chem. Res. 2014, 53, 6325−6333

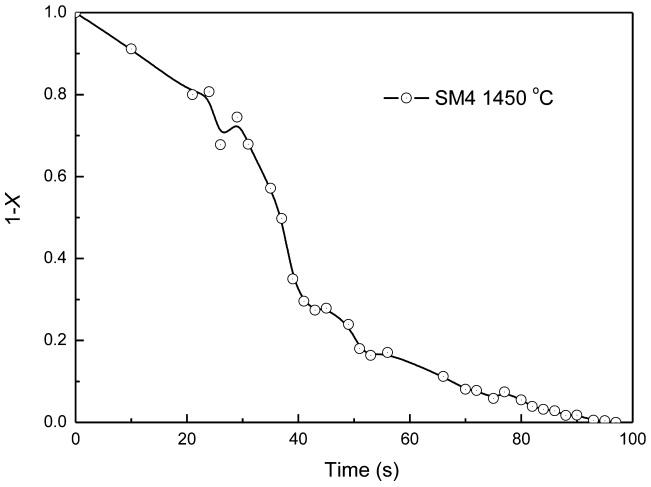

Figure 2. Typical dissolution profile of a lime particle in a CaO–Al_2O_3–SiO_2-based slag with recorded particle size reclamation (slag SM4 at 1450 °C).

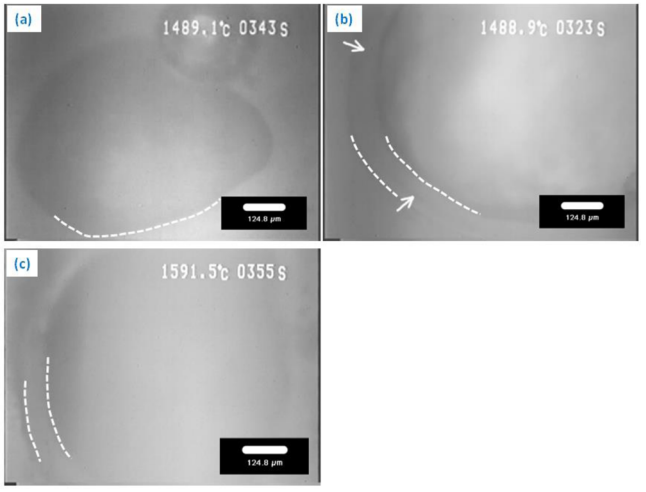

Figure 3. IR layer formed during CaO dissolved in slag without MgO and comparison with dissolution in slag with MgO: (a) slag SM4, (b) slag SM04,[13] and (c) slag SM04 at higher temperature.

(compare Figure 3a, b, and c). The *in situ* observation showed that this layer formed after the CaO particle had been immersed into the molten slag for a certain time, suggesting an accumulation period for its formation. The layer grew with time, reaching a maximum thickness. Afterward, it dissolved into the slag, faded, and finally disappeared. The remaining lime then dissolved at a rapid rate (see Movie 2).

The nature of the IR layer has been discussed in our previous paper, and a smaller compositional range of CaO for solid precipitation is believed to play an important role.[13] In order to have a better understanding of the formation mechanisms of the IR layer, the phase diagrams of the slag systems involved were calculated by using FactSage software (version 6.2) with the FToxid database and compared with ref 15, as shown in Figure 4. During dissolution, a concentration gradient of CaO would be built between the slag bulk and CaO particles (blue dashed lines indicate the compositional distance between each slag to the boundary of CaO primary phase field). The dissolution path of CaO at a certain temperature and in a given slag would pass through the phase transition zones in the concentration range constrained by the composition of the bulk (slag) and CaO content in the particle (100 wt % CaO). However, this argument is a simplification, and the dissolution path or the phases formed during dissolution may vary with experimental conditions. Because the dissolution process is not always in equilibrium, the phase transformation may not necessarily follow the phase diagram in Figure 4, and compositions of the primary solid phases may also be different. In order to reach an easier comparison of the kinetics in different slags, the simplification of the dissolution path shown in Figure 4 can be helpful. In the present case of quiescent or low Reynolds number ($Re \ll 1$) melt flow, the phases that may precipitate adjacent to the particle can be approximately predicted by the phase diagrams in Figure 4. Considering CaO dissolved in slag SM01 at 1600 °C (Figure 4a), $2CaO{\cdot}SiO_2$ and $3CaO{\cdot}SiO_2$ may form adjacent to the CaO particle (Figure 4(a), and they have been identified in our previous research.[13] It can be concluded that the CaO concentration range in the slag is very wide for solid precipitation (Figure 4a) compared with the range for slags containing 10 wt % MgO. The visible IR layer shown in Figure 3 should be the precipitation of solid phases around the particle during dissolution, and this layer may have a tendency to inhibit further dissolution of lime.[8]

In the slags containing MgO, no IR layer was observed at the experimental temperatures. Compared with the MgO-free slags, the range of CaO concentration for solid precipitation (from the liquidus boundary at a certain temperature to the primary phase field boundary of CaO) is substantially narrow. When solid phases precipitate, they can be easily dissolved by the slags and become invisible. The existence of the IR layer is also believed to be influenced by the local mass transfer condition. To illustrate this effect, the slag viscosity was calculated at different temperatures by using the model developed by Riboud.[15] By comparing the data shown in Table 2, an obvious conclusion can be drawn that the addition of MgO can significantly lower slag viscosity. With improved fluidity, enhanced diffusion/mass transfer and thinner boundary layer in such slags would be expected. Consequently, the solid phases precipitated adjacent to the lime particle could be redissolved into the slags rather than forming the IR layer (Figure 2S, Supporting Information).

Although the calculated phase diagrams in Figure 4 provide reasonable explanations on the formation of the IR layer, shortcomings need to be addressed: (1) Because the lime dissolution is fast and the stable equilibrium is hard to reach, the prediction of new phases and dissolution path may bring deviation.[16] (2) The precipitation of new phases would cause compositional divergence in the slags, especially causing depleted zones of SiO_2, Al_2O_3, and/or MgO near the particle. The precipitated phases may differ from what are predicted via thermodynamic equilibrium (Figure 4). In this case, the dissolution kinetics on the other hand becomes essential supplements in understanding the actual dissolution mechanisms.

3.3. Dissolution Mechanisms and Kinetics. Lime dissolution mechanisms are associated with its dissolution path during dissolution. To investigate the dissolution mechanisms, the classical shrinking core model[17] was applied, and experimental results were compared to those predicted by the model. A typical dissolution without the formation of a solid product layer around the lime particle includes three steps: (1) diffusion (mass transfer) of reactant from the bulk through the boundary layer to the surface of the solid, (2) chemical reactions at the interface between reactant and solid, and

dx.doi.org/10.1021/ie500070h | Ind. Eng. Chem. Res. 2014, 53, 6325–6333

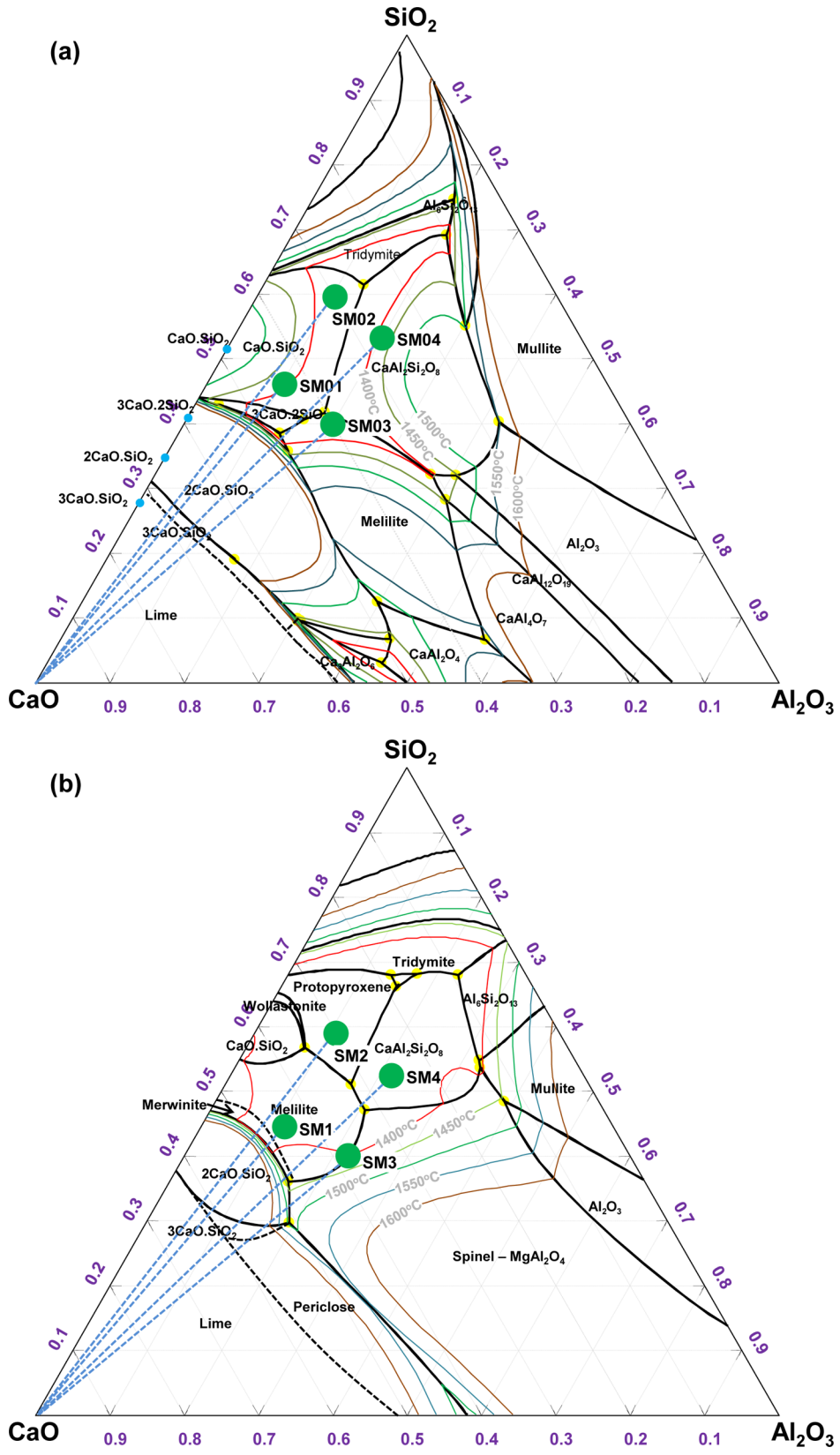

Figure 4. Calculated phase diagrams with FactSage 6.2 for the CaO–Al_2O_3–SiO_2-based slags: (a) slags without MgO content, (b) slags with 10 wt % MgO. Black dashed lines indicate additional primary phase field boundaries according to ref 15.

(3) diffusion of the reaction product from the interface into the bulk through the boundary layer. If a firm product forms outside the solid particle, the diffusion of reactant and/or product through the solid product layer must be taken into account. The step with the highest resistance is considered to be rate controlling.

dx.doi.org/10.1021/ie500070h | *Ind. Eng. Chem. Res.* 2014, 53, 6325–6333

Table 2. Viscosity (Pa s) of Slags at Different Temperatures

slag number	1450 °C	1500 °C	1550 °C	1600 °C
SM01	1.12	0.79	0.57	0.41
SM02	7.77	5.14	3.48	2.40
SM03	2.37	1.54	1.02	0.70
SM04	14.57	8.92	5.62	3.63
SM1	0.46	0.34	0.25	0.19
SM2	2.36	1.63	1.14	0.82
SM3	0.90	0.61	0.42	0.30
SM4	4.10	2.63	1.73	1.16

Under the assumption of chemical reactions at the interface controlling process, a relation between the fractional conversion X and the fractional dissolution time is obtained as

$$1 - X = \left(1 - \frac{t}{\tau}\right)^3 \tag{1}$$

where t and τ are the actual time and total dissolution time, respectively, and X is the fractional conversion given by

$$X = 1 - \left(\frac{r}{r_0}\right)^3 \tag{2}$$

where r and r_0 are the actual and initial particle size, respectively.

If the dissolution is controlled by boundary layer diffusion (in the Stokes regime), the conversion in terms of the fractional time for complete dissolution is described as

$$1 - X = \left(1 - \frac{t}{\tau}\right)^{3/2} \tag{3}$$

If the resistance to diffusion through the product layer controls the reaction rate, the progression of reaction in terms of fractional conversion will become

$$\frac{t}{\tau} = 1 - 3(1 - X)^{2/3} + 2(1 - X) \tag{4}$$

For comparison, two typical CaO dissolution curves in slags with and without the formation of an IR layer are shown in Figure 5a with open circles and triangles, respectively. The theoretical calculations for different rate-controlling steps are contemporarily plotted, i.e., solid line for chemical reaction control (eq 1), dashed line for boundary layer diffusion control (eq 3), and dashed dotted line for product layer diffusion (eq 4). When the slag contains MgO (SM2, Figure 5a, with open triangle), the dissolution profile fits well with the solid line, indicating that the process is controlled by chemical reactions at the solid/liquid interface. However, the dissolution profile in the slag without MgO (SM02, Figure 5a, with open circle) becomes complex, corresponding to theoretical calculations, and none of them is fitted. The existence of the IR layer in Figure 3 is believed to be the reason for this variance. By associating the dissolution profile in Figure 5a with the in situ observation (see Movie 2), it was found that the dissolution process can be divided into three stages, i.e., early, intermediate, and late. The early stage constitutes the accumulation period of forming a layered structure, during which the dissolution rate is relatively fast. The intermediate stage starts as soon as the IR layer has arisen. The particle dissolves with the lowest dissolution rate at this stage. The late stage commences when the IR layer disappears completely, and the dissolution becomes faster again. The radius evolution of the lime particle at each stage is represented by fractional conversion $(1 - X)$ against the dimensionless time in Figure 5b for slag SM02 at 1600 °C separately. It is clear that the dissolution is chemical reaction-controlled in the early stage. After an additional layer is formed, the dissolution is controlled by the diffusion in the product layer in the intermediate stage. At the late stage, diffusion/mass transfer in the boundary layer becomes the largest resistance for the dissolution.

To sum up, dissolution of lime particles in $CaO–Al_2O_3–SiO_2$ slags shows a higher degree of complexity when the IR layer forms. The dissolution rate is further influenced by temperature, physiochemical properties, and composition of the slag, and the spans of different stages vary at different dissolution conditions. In the following, the effects of different factors on the dissolution are systematically discussed.

3.4. Resistance and Driving Force during Lime Dissolution. The dissolution rate at any instant can be expressed as[17]

$$-\frac{dn_{CaO}}{dt} = \frac{4\pi r^2}{\frac{1}{k_d} + \frac{r_0(r_0 - r)}{D_{eff} r} + \frac{1}{k_r}}(C^s_{CaO} - C^b_{CaO}) \tag{5}$$

where n_{CaO} is the mole number of CaO, k_d, D_{eff}, and k_r are, respectively, the mass transfer coefficient, effective diffusion coefficient, and reaction rate constant (reaction CaO(s) → (CaO)),

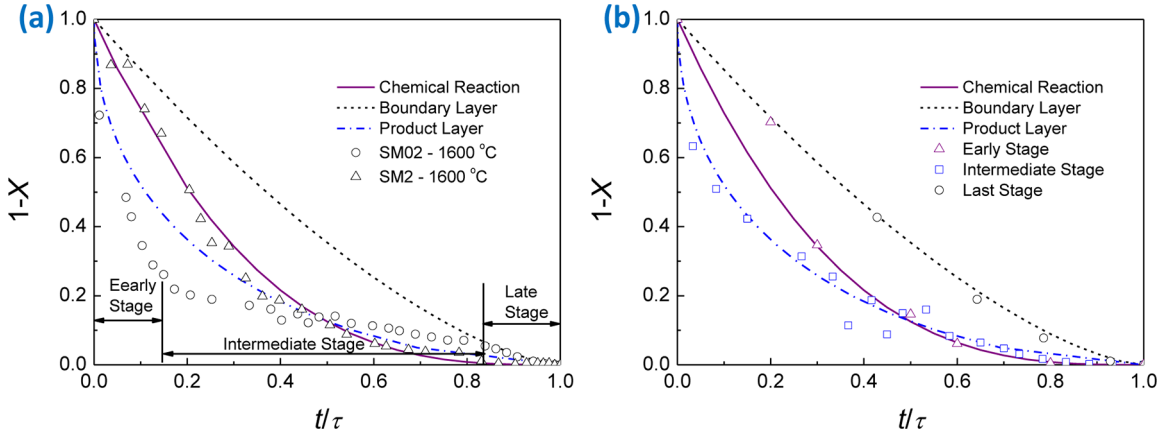

Figure 5. Dissolution curves of CaO in slag SM02 at 1600 °C and in SM2 at 1600 °C: (a) comparison of different slags and (b) comparison of different stages (SM02).

dx.doi.org/10.1021/ie500070h | Ind. Eng. Chem. Res. 2014, 53, 6325−6333

and C^{s}_{CaO} and C^{b}_{CaO} are the concentration of CaO, respectively, at the interface between the CaO particle and the molten slag and in the bulk of the slag. The CaO concentration at the interface can be obtained in corresponding phase diagrams calculated by FactSage software under the assumption of local equilibrium. The term $1/k_t = 1/k_d + (r_0(r_0 - r))/(D_{eff}r) + 1/k_r$ represents the total resistance against the dissolution, and the term $\Delta C_{CaO} = (C^{s}_{CaO} - C^{b}_{CaO})$ corresponds to the driving force of the reaction.

Table 3 represents the driving force of lime dissolution for each slag. The driving force, being indicated by the open arrows

Table 3. Initial Driving Force of Lime Dissolution for Each Slag at Different Temperatures, ΔC_{CaO} (mol/L)

slag number	1450 °C	1500 °C	1550 °C	1600 °C
SM01	3.26	3.47	3.71	3.98
SM02	11.75	11.89	12.07	12.27
SM03	4.53	4.67	4.95	5.28
SM04	11.80	11.98	12.19	12.44
SM1	2.13	2.31	2.54	2.80
SM2	9.95	10.08	10.23	10.42
SM3	2.05	5.46	5.99	6.64
SM4	11.02	11.25	11.53	11.86

in Figure 4a, increases with temperature. The magnitude of ΔC_{CaO} depends significantly on the phase evolution and slag compositions. However, the effect of adding MgO in the slag on the driving force is trivial (Table 3).

The resistance to lime dissolution comprises mass transfer, diffusion, and chemical reactions based on eq 5. Regarding the resistance, a quantitative description of each parameter can be given by the following equations. The reaction rate constant k_r shows Arrhenius behavior with temperature,[17] and namely, increasing temperature results in higher k_r values.

$$k_r = A_r \exp\left(\frac{-E_a}{RT}\right) \tag{6}$$

is where E_a is the activation energy, R the gas constant, A_r is the pre-exponential factor, and T is the temperature.

The mass transfer coefficient is related to the diffusion coefficient D in the Stokes regime (with very low Reynolds number) via[17]

$$k_d = C\frac{D}{r} \tag{7}$$

where C is a constant, and r is the characteristic length of the diffusion path of CaO.

The diffusion coefficient D is associated with the viscosity of slag by the Eyring relation[18]

$$D = \frac{k_b T}{\eta \lambda} \tag{8}$$

where k_b is the Boltzmann constant, η is the viscosity of slag, and λ is the jump distance.

Diffusion through the product layer is different from free diffusion and can be related to the diffusion coefficient by considering the porosity (ε_p) of the product layer and sinuosity (s) of the diffusion path,[19]

$$D_{eff} = \frac{D\varepsilon_p}{s} \tag{9}$$

Assuming that the spatial structures through the product layers during dissolution in different slags are the same and ε_p/s has identical values, the effective diffusion coefficient D_{eff} is directly correlated with the diffusion coefficient of CaO.

Effect of Temperature on Lime Dissolution. According to eqs 7 and 8, the mass transfer coefficient k_d is proportional to temperature and inversely proportional to viscosity. The viscosity of each slag decreases at a higher temperature as shown in Table 2. It can be deduced that the mass transfer coefficient increases with temperature. Chemical reactions and diffusion are also temperature sensitive, and the dissolution kinetics can therefore be largely influenced by temperature.

Figure 6 illustrates the dissolution profiles of lime in slag SM02 at different temperatures. The dissolution rate increases

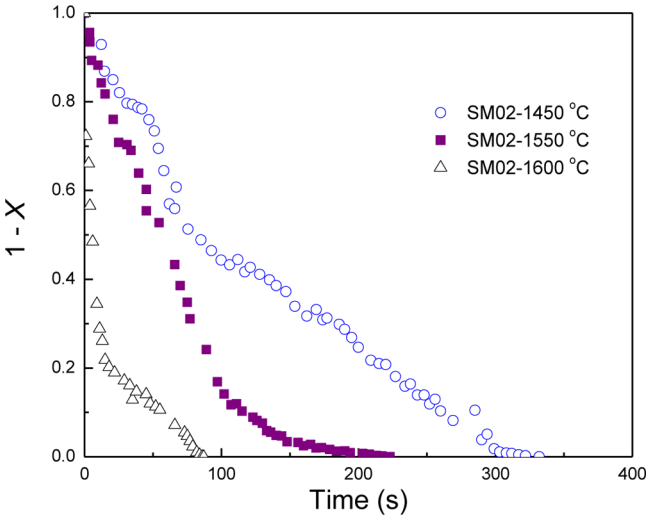

Figure 6. Dissolution curves of CaO in slag SM02 at different temperatures.

with temperature, and this increase is more significant at the earlier stages of dissolution. It indicates that in these stages, the resistance during dissolution is effectively decreased by increasing the temperature,which is in line with eqs 6–8 (temperature dependent).

As shown in eq 5, the dissolution rate is also significantly influenced by the dissolution driving force, ΔC_{CaO}. The driving force is raised with temperature as demonstrated in Table 3. The reason is that the saturation concentration of CaO increases with temperature in all slags, while the CaO content in the bulk stays the same. The increase in the driving force with temperature provides substantial contribution to enhance the dissolution.

Effect of Slag Basicity (B) on Lime Dissolution. Figure 7 compares the dissolution profiles of slags with different basicity (0.5 and 1.0). It shows that CaO dissolved faster in slags with basicity of 0.5 (Figure 7). This can be explained by considering both contributions: dissolution driving force and resistance. The driving force for slags with smaller basicity is always larger as shown in Table 3.

A Factor Coupling the Driving Force and the Resistance. For the slags with MgO, the rate-controlling step for lime dissolution is the mass transfer of CaO through the boundary layer (Figure 5(a). However, the dissolution is complicated for the slags without MgO addition, and a stepwise rate-controlling step is realized (Figure 5b). Meanwhile, Figure 3S

dx.doi.org/10.1021/ie500070h | Ind. Eng. Chem. Res. 2014, 53, 6325–6333

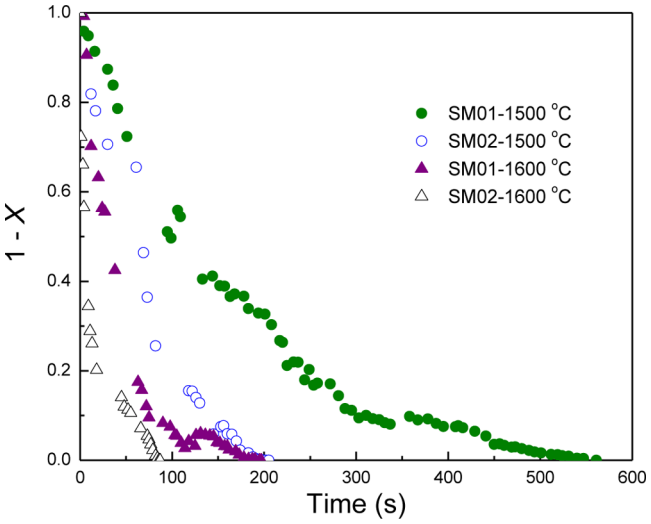

Figure 7. Effect of basicity on dissolution of CaO in slags without MgO addition.

of the Supporting Information gives the lime dissolution profiles fitting the different rate-controlling steps in the example of slags with MgO. It can be found that the dissolution controlling step varies at different slag compositions and temperature. Therefore, it makes direct comparison between the two types of slags (with and without MgO) difficult. By comparing the rate control of lime dissolution at different steps for slags without MgO (Figure 5(a)), it is found that the period of the early stage dissolution, which is chemical reaction controlled, is short. If only considering the intermediate and late stages, the dissolution depends directly on the diffusion coefficient and the driving force (neglecting the k_r term in eq 5) according to eqs 5−9. The factors that influence the lime dissolution in all slags include the driving force, viscosity, and temperature. Therefore, a dissolution factor $\Delta C_{CaO}/\eta^{20}$ is defined to evaluate and compare the dissolutions in different slags.

As shown in Figure 8, $\Delta C_{CaO}/\eta$ varies with slag compositions and increases with temperature. By evaluating the $\Delta C_{CaO}/\eta$ values in Figure 8, they are correlated to the experimental results in Figures 5−7. It is found that a larger $\Delta C_{CaO}/\eta$ value gives a larger dissolution rate or slope of the dissolution profiles. An example is given in Figure 8a and b for slag SM02. It illustrates that the relative dissolution time (defined as the total dissolution time divided by the starting lime particle volume prior to dissolution into slag t_T/V_P) decreases with the dissolution factor. Therefore, this factor can explicitly represent the capacity of lime dissolution in different slags. For the slags without MgO content, $\Delta C_{CaO}/\eta$ shows a tendency of monotonic increase indicating a higher dissolution rate with an increase in CaO content in the slags and temperature. When the slags contain MgO, a different phenomenon for SM3 is found. The $\Delta C_{CaO}/\eta$ value is the lowest at lower temperature, i.e., 1450 °C, while it increases dramatically with temperature and becomes the highest from 1500 °C (Figure 8c). This phenomenon can be well explained by the phase diagram of slag SM3 in Figure 4g. At 1450 °C, the presence of melilite and spinel phases in the liquid slag inhibits lime dissolution, and the

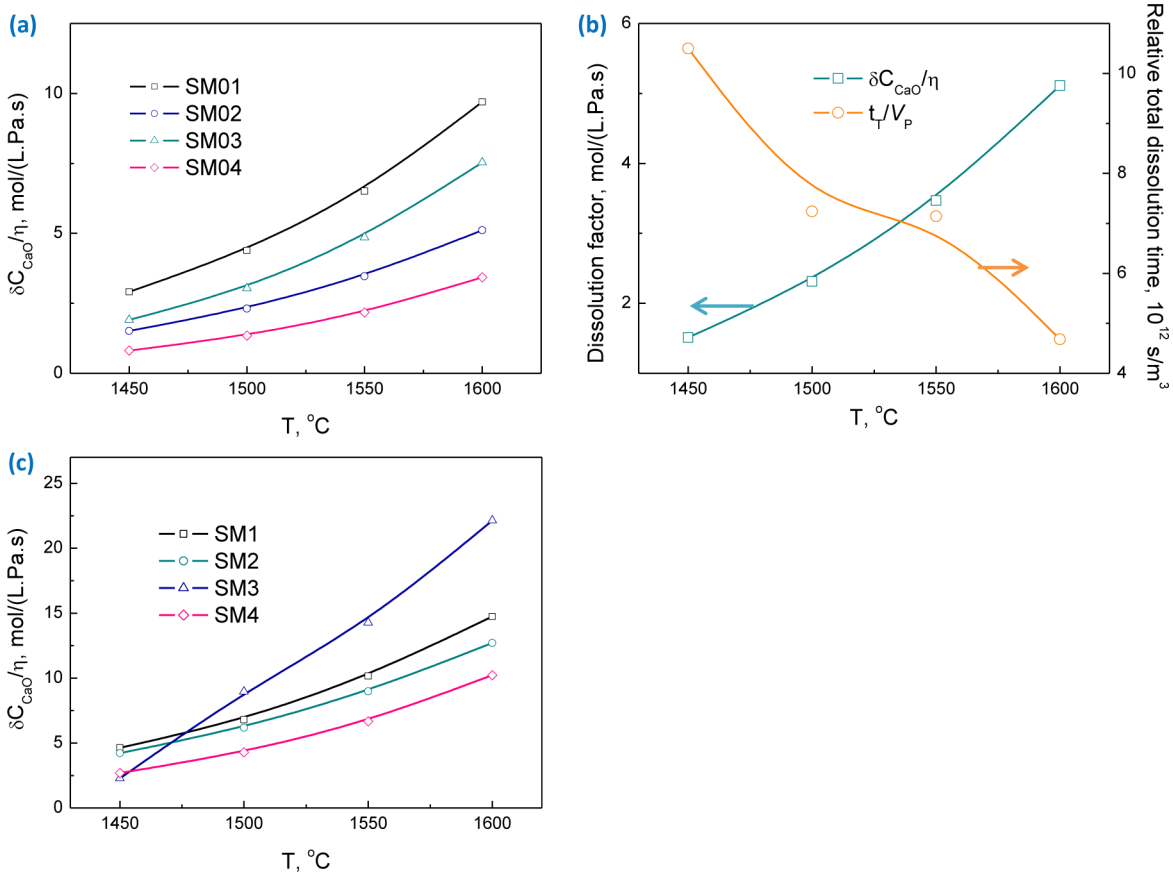

Figure 8. Temperature dependence of $\Delta C_{CaO}/\eta$ for different slags: (a) without MgO addition, (b) indication of shorter dissolution time with larger dissolution factor at different temperatures for slag SM02, and (c) with MgO addition.

dx.doi.org/10.1021/ie500070h | Ind. Eng. Chem. Res. 2014, 53, 6325−6333

driving force is very low (Table 3). When the temperature reaches 1500 °C, the liquid−spinel and liquid−melilite region disappear, and the driving force for lime dissolution is more than twice that at 1450 °C. This contributes an increase in the $\Delta C_{CaO}/\eta$ value. With the addition of MgO, the values of the dissolution factor increase significantly by comparing Figure 8a and c. It can be increased by one or two times for slags with the same CaO to SiO_2 ratio by adding 10 wt % MgO. The main reason comes from a remarkable reduction of the slag viscosity. The presence of MgO in the slag contributes to depolymerize the Si−O structure, leading to a lower viscosity.[21]

3.5. Practical Consideration. According to the above discussion, it has been revealed that lime dissolution exhibits distinct mechanisms in liquid slags with and without MgO. The addition of MgO effectively eliminates IR layer formation by narrowing the solid precipitation range (Figure 4). Figure 9 gives a direct comparison of the dissolution profiles in liquid slags with and without MgO at 1450 °C. By comparing the two dissolution profiles of slags SM04 and SM4, the dissolution rates at the intermediate and late stages are evidently improved in slag SM4 with MgO addition. It allows for a faster dissolution of lime during primary steelmaking. On the other hand, steelmaking operations require an appropriate slag viscosity, which directly influences tap-to-tap time, slag foaming, and refractory lifetime. As shown in Table 2, the slag viscosity varies with slag composition, and MgO addition effectively decreases the viscosity of the slags, which provides evidence that dolomite flux (e.g., $CaMg(CO_3)_2$) used in BOF and EAF practices is beneficial for both lime dissolution and slag viscosity control. Additionally, the quantitative understanding of lime dissolution in $CaO-SiO_2-Al_2O_3$-based slags may be easily extended to predict the behavior of other monoxide additions, e.g., FeO and TiO_2. It is also clear that the apparent dissolution rate is influenced by other factors such as lime particle size, flow field related to gas stirring, and other oxides in the slags that requires further investigation.

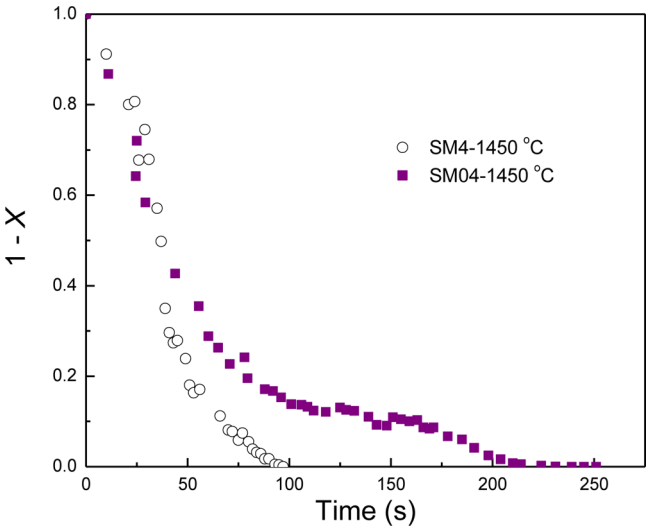

Figure 9. Effect of MgO content in the slag on dissolution of CaO.

4. CONCLUSIONS

The dissolution of CaO particles in $CaO-Al_2O_3-SiO_2$-based slags with and without MgO has been investigated using a confocal scanning laser microscope (CSLM) between 1450 and 1600 °C. An obvious IR layer was observed during CaO dissolution in slags free of MgO. This causes the rate-controlling step to shift from diffusion in the boundary layer to a mixed regime of chemical reactions at the interface and diffusion in the boundary layer and the product layer. The IR layer was not observed in slags with MgO addition owing to the lower viscosity and the narrower concentration range for IR layer formation. The resistance and driving forces of lime dissolution in different slags were discussed with respect to the effects of temperature and basicity. A dissolution factor $\Delta C_{CaO}/\eta$ was defined. It was found that a larger $\Delta C_{CaO}/\eta$ value gives a larger dissolution rate or the slope of the dissolution profiles. The benefit/significance of MgO addition allows for faster dissolution of lime during primary steelmaking.

■ ASSOCIATED CONTENT

Ⓢ Supporting Information

Figures about temperature calibration of the CSLM, SEM images of the product layer formation, and fitting of experimental results with different kinetics models. This material is available free of charge via the Internet at http://pubs.acs.org.

Ⓦ Web-Enhanced Features

Movies 1 and 2 indicate the lime dissolution process at different conditions. They are available in the HTML version of the paper.

■ AUTHOR INFORMATION

Corresponding Authors

*E-mail: zhisun@126.com (Z.H.I.S.).
*E-mail: muxing.guo@mtm.kuleuven.be (M.G.).

Present Addresses

X. Guo: Department of Materials Science and Engineering, TU Delft, 2628 CD Delft, The Netherlands.
Z. H. I. Sun: Department of Materials Science and Engineering, TU Delft, 2628 CD Delft, The Netherlands.

Notes

The authors declare no competing financial interest.

■ ACKNOWLEDGMENTS

The authors acknowledge Dr. F. Verhaeghe for constructive discussion. The authors also gratefully acknowledge the contribution of the anonymous reviewers whose expertise helped to improve the manuscript.

■ REFERENCES

(1) Fruehan, R. Desulfurization of liquid steel containing aluminum or silicon with lime. *Metall. Mater. Trans. B* **1978**, *9*, 287−292.
(2) Hamano, T.; Fukagai, S.; Tsukihashi, F. Reaction mechanism between solid CaO and $FeO_x-CaO-SiO_2-P_2O_5$ slag at 1573 K. *ISIJ Int.* **2006**, *46*, 490−495.
(3) Sun, Z.; Zhang, Y.; Zheng, S.-L.; Zhang, Y. A new method of potassium chromate production from chromite and $KOH-KNO_3-H_2O$ binary submolten salt system. *AlChE J.* **2009**, *55*, 2646−2656.
(4) Amini, S.; Brungs, M.; Ostrovski, O.; Jahanshani, S. Effects of additives and temperature on dissolution rate and diffusivity of lime in $Al_2O_3-CaO-SiO_2$ based slags. *Metall. Mater. Trans. B* **2006**, *37*, 773−780.
(5) Deng, T.; Gran, J.; Sichen, D. Dissolution of lime in synthetic $FeO-SiO_2$ and $CaO-FeO-SiO_2$ slags. *Steel Res. Int.* **2010**, *81*, 347−355.

(6) Elliott, L. K.; Lucas, J. A.; Happ, J.; Patterson, J.; Hurst, H.; Wall, T. F. Rate limitations of lime dissolution into coal ash slag. *Energy Fuels* **2008**, *22*, 3626−3630.
(7) Guo, M.; Parada, S.; Jones, P. T.; Boydens, E.; Dyck, J. V.; Blanpain, B.; Wollants, P. Interaction of Al_2O_3-rich slag with MgO−C refractories during VOD refining—MgO and spinel layer formation at the slag/refractory interface. *J. Eur. Ceram. Soc.* **2009**, *29*, 1053−1060.
(8) Yang, J.; Kuwabara, M.; Asano, T.; Chuma, A.; Du, J. Effect of lime particle size on melting behavior of lime-containing flux. *ISIJ Int.* **2007**, *47*, 1401−1408.
(9) Lee, S. H.; Tse, C.; Yi, K. W.; Misra, P.; Chevrier, V.; Orrling, C.; Sridhar, S.; Cramb, A. W. Separation and dissolution of Al_2O_3 inclusions at slag/metal interfaces. *J. Non-Cryst. Solids* **2001**, *282*, 41−48.
(10) Kim, J. H.; Kim, S. G.; Inoue, A. In situ observation of solidification behavior in undercooled Pd-Cu-Ni-P alloy by using a confocal scanning laser microscope. *Acta Mater.* **2001**, *49*, 615−622.
(11) Liu, J.; Verhaeghe, F.; Guo, M.; Blanpain, B.; Wollants, P. In situ observation of the dissolution of spherical alumina particles in CaO−Al_2O_3−SiO_2 melts. *J. Am. Ceram. Soc.* **2007**, *90*, 3818−3824.
(12) Fox, A. B.; Valdez, M. E.; Gisby, J.; Atwood, R. C.; Lee, P. D.; Sridhar, S. Dissolution of ZrO_2, Al_2O_3, MgO and $MgAl_2O_4$ particles in a B_2O_3 containing commercial fluoride-free mould slag. *ISIJ Int.* **2004**, *44*, 836−845.
(13) Sun, Z. H. I.; Guo, X.; Van Dyck, J.; Guo, M.; Blanpain, B. Phase evolution and nature of oxide dissolution in metallurgical slags. *AlChE J.* **2013**, *8*, 2907−2916.
(14) Liu, J.; Guo, M.; Jones, P. T.; Verhaeghe, F.; Blanpain, B.; Wollants, P. In situ observation of the direct and indirect dissolution of MgO particles in CaO−Al_2O_3−SiO_2-based slags. *J. Eur. Ceram. Soc.* **2007**, *27*, 1961−1972.
(15) Eisenhüttenleute, V. D. *Slag Atlas*; Verlag Stahleisen: Düsseldorf, 1995.
(16) Soll-Morris, H.; Sawyer, C.; Zhang, Z. T.; Shannon, G. N.; Nakano, J.; Sridhar, S. The interaction of spherical Al_2O_3 particles with molten Al_2O_3−CaO−FeO_x−SiO_2 slags. *Fuel* **2009**, *88*, 670−682.
(17) Levenspiel, O. *Chemical Reaction Engineering*, 3rd ed.; John Wiley & Sons: New York, 1999.
(18) Poirier, D. R.; Geiger, G. H. *Transport Phenomena in Materials Processing*; TMS: Warrendale, PA, 1994.
(19) Li, W. *Physical Chemistry of Metallurgy and Materials*; Metallurgical Industry Press: Beijing, 2001.
(20) Elliott, L.; Wang, S. M.; Wall, T.; Novak, F.; Lucas, J.; Hurst, H.; Patterson, J.; Happ, J. Dissolution of lime into synthetic coal ash slags. *Fuel Process. Technol.* **1998**, *56*, 45−53.
(21) Kim, H.; Kim, W. H.; Sohn, I.; Min, D. J. The effect of MgO on the viscosity of the CaO−SiO_2−20 wt%Al_2O_3−MgO slag system. *Steel Res. Int.* **2010**, *81*, 261−264.